Materials Today: Proceedings 44 (2021) 3467–3474

Contents lists available at ScienceDirect

Materials Today: Proceedings

journal homepage: www.elsevier.com/locate/matpr

Performance evaluation and stability of silicide-based thermoelectric modules

Antoine de Padoue Shyikira [a,*], Gustein Skomedal [a,b], Peter Hugh Middleton [a]

[a] University of Agder, Norway
[b] Elkem ASA – Kristiansand, Norway

ARTICLE INFO

Article history:
Received 21 October 2019
Received in revised form 26 April 2020
Accepted 7 May 2020
Available online 12 June 2020

Keywords:
Thermoelectric module
Silicides
Degradation
Stability

ABSTRACT

Long-term studies on thermoelectric generators based on N-type magnesium silicide ($Mg_{2.01}Si_{0.49}Sn_{0.5}Sb_{0.01}$) and P-type higher manganese silicide ($Mn_{0.98}Mo_{0.02}Si_{1.73}Ge_{0.02}$) materials are presented, in the operating temperature range of 200 °C–400 °C. Emphasis is put on the performance and reliability of the current collector configuration, especially on the hot side of the module, and on the thermomechanical stresses that are created during operation and lifetime testing as a result of large temperature gradients experienced across the thermoelectric legs. With silver (Ag) paste as contact material, the long term-stability of the uni-couples was carried out on non-metalized legs and gold metalized legs under ambient conditions. Under isothermal and thermocycling tests, the non-metalized legs showed a gradual decrease in open circuit voltage (after a period of 200 h) and increase in internal resistance. Conversely, the module made of metalized legs was robust and stable for the same isothermal period. However, after 300cycles the n-type material showed mechanical failure (cracks) but the p-type resisted. Post-operation analysis by SEM/EDS and mechanical testing revealed that oxidation, adherence of the contact material and diffusion of the bonding material were the cause of performance degradation of the unicouples.

1. Introduction

Silicide-based thermoelectric materials (TEM) are promising materials for the future of thermoelectrics. These materials are among the best candidates for mass production [1], due to high abundancy of raw materials in the earth crust (especially silicon 2nd, magnesium 8th and manganese 12th [2]), low cost and non-toxicity. For a long time, ($Si_{1-x}Ge_x$) was proven to be good for thermoelectric application in radioisotopes thermoelectric generators [3], though new compounds were proposed and studied, including compounds based on higher manganese silicide (HMS) [4,5] and magnesium silicide (MGS). These compounds have shown good transport properties, with figures of merit around 0.6 and 1.5, respectively, and more research is still being carried out to optimize the transport properties. Moreover, coupling of HMS and MGS in a module was proposed by many researchers for terrestrial application [6,7,8], though the combination has not been implemented in any of the modules on the market.

Today, more research has focused at the materials level, improving the transport properties, figure of merit and the mechanical properties. However, not much research has been done at the module level, especially on the MGS-HMS combination, and even less work has been conducted on electrodes and electrode-TEM interfaces. Previous work from our group Skomedal et al. [6], worked on modelling, designing, assembling HMS (p-type) – MGS (n-type) modules and testing their performance and stability over time. The three unicouples used in the module showed good performance, which reached a peak power of 3.24 W at a hot side temperature of 735 °C, and 1.04 W maximum power at 405 °C. Moreover, Nakamura et al. [9], studied a π shaped module based on Mg_2Si and $MnSi_{1.73}$, as n- and p-type TEMs, respectively. With Ag electrode, Ag bonding material and Ni diffusion barrier, their module produced 4.4 kW/m^2 at 548 °C. However, both Skomedal and Nakamura's modules degraded during thermal cycles mainly due to oxidation of the MGS, and coefficient of thermal expansion (CTE) mismatches at the bonding interface. By contrast, De Boor et al. [10], has investigated the stability of Mg_2Si and nickel electrode contact. The contact was successfully formed by mutual sintering the TEM and the electrode (at 1123 K), which resulted in a 10–30 μm Mg-Si-Ni reaction layer. The study was done under

* Corresponding author.
E-mail addresses: antoine.d.shyikira@uia.no, tonnydepadoue15@gmail.com (A.P. Shyikira).

https://doi.org/10.1016/j.matpr.2020.05.193
2214-7853/

isothermal treatment for 168 h at 823 K and no cracks were observed by SEM, which the authors claim was a result of a relatively thick contact layer that also hindered diffusion of Mg to the Ni side. However, they recommend thermal cycle runs to investigate and confirm the reliability of Mg_2Si -Ni contact.

Kaibe et al. [11], studied cascaded modules made of p-Mn-Si and n-Mg-Si on the hot side and Bi-Te base alloys on the cold side with which they achieved 12% efficiency at 550 °C. Their results were promising, though the stability of the cascaded module remained an issue due to complex chemical phenomena occurring overtime, from electrodes (Ni-plated Cu electrodes) to bonding materials involving oxidation and intermetallic diffusion which should be investigated. Similarly, Hee Seok Kim et al. [7], studied a segmented TE module, with MGS(Mg_2Si) – HMS ($MnSi_{2-x}$, x = 0.25–0.273) mounted on top at the high temperature segment and n- and p- type Bi-Te module on the cold side. Contact electrodes were made from Cu on both the hot side and cold side, with 50 nm Ti and 1 μm Ag layers. Under isothermal heat treatment between 23 and 520 °C for 30 h, they achieved a contact resistance of 50μΩcm^2 and a contact resistance to total module resistance ratio of 2%, moreover, they achieved a specific power density of 42.9 W/kg with a 498 °C temperature difference. Among other possibilities, Ni and Ag electrodes [10,12–15], Cu electrodes [7,14], and molybdenum (Mo) [6] have been mostly studied. It seems, from the aforementioned electrodes that Ag was the most reliable followed by Ni, with around 10μΩcm^2 vs 25-5010μΩcm^2 specific resistance on MGS [10,12].

Some of the key factors that affect performance and stability over time for TE modules are diffusion at the electrode/bonding material – TEM interface, bonding strength and contact resistance. At module contacts, diffusion is a deteriorative factor, however, as reported by Liu et al. [16], it is also important to note that limited diffusion is important for crack free contacts. However, diffusion during operation should be avoided as, in some cases diffusion can alter the doping and turn an n-type into a p-type TEM; this would seriously shorten the in-service lifetime of the device. Altering the doping would reduce the charge carrier concentration and affect the performance of the module by lifetime shortage or reduction of the mechanical reliability. So apart from the strong bond through diffusion, a diffusion barrier is also important to stop further diffusion during operation. Moreover, a strong and reliable bond requires good matching of the coefficient of thermal expansion (CTE) of the electrode and the TEM. In the current study, the CTE for a mixture of phases has been approximated using a model by Karunaratne M.S.A. et al. [17] equation 1, where, $\bar{\alpha}, \omega_i, \rho_i, \bar{\alpha}_i$ stand for the CTE of the alloy/mixture, the weight fraction of phase i, the density of phase i, and the CTE of individual phase i.

$$\bar{\alpha} = \frac{\sum \bar{\alpha}_i \{\omega_i/\rho_i\}}{\sum \{\omega_i/\rho_i\}} \quad (1)$$

It is difficult to model thermal contact resistance as it requires coupling the phonons carrying heat from the heating element through the interface to the TE leg. Well-known models include the acoustic mismatch model and the diffusive mismatch model [18]. However, the modern molecular dynamic simulation [19] suggested that the phonons at the interface scatters as a mixture of acoustic scattering and diffusive scattering, so the bond strength is a deterministic factor of the interface contact resistance. Therefore, if the coefficients of thermal expansion (CTE) of the materials is closely matched, a good contact can be achieved by sintering them together to allow diffusion to take place and therefore a strong bond developed. However, the materials reactivity level towards higher temperatures and the stability of the bond over high thermal stress, operational diffusion passivation, high electrical, chemical and thermal conductivity are the next challenges to overcome.

2. Materials and methods

2.1. Materials and modules

The uni-couple modules were assembled using MGS ($Mg_{2.01}Si_{0.49}Sn_{0.5}Sb_{0.01}$) as n-type and HMS ($Mn_{0.98}Mo_{0.02}Si_{1.73}Ge_{0.02}$) as p-type. The powder materials used in this research are synthesized

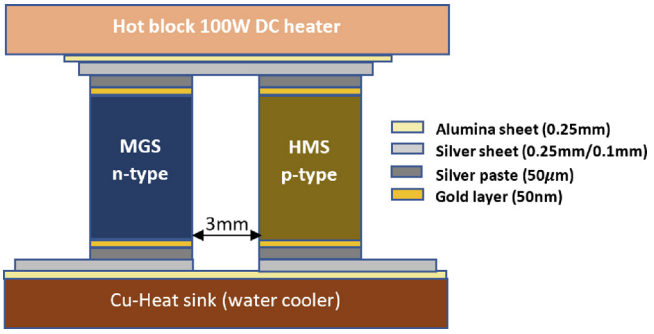

Fig. 1. A detailed schematic representation of a unicouple module test-assembly.

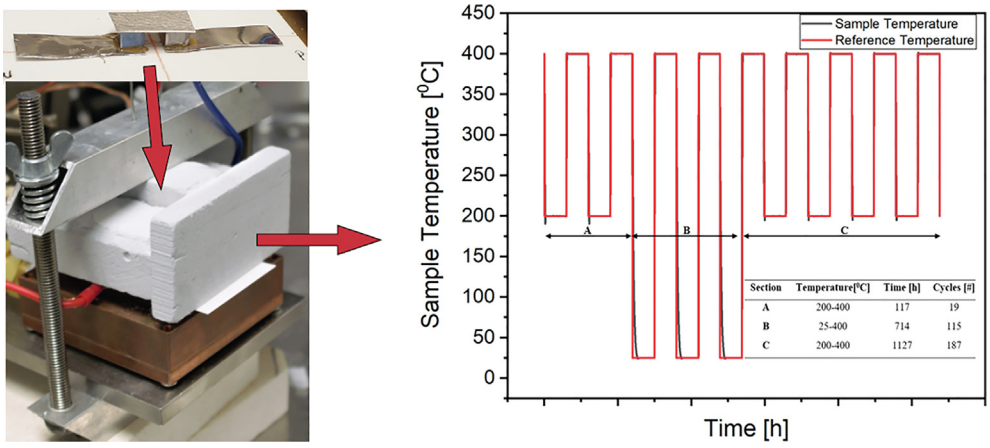

Fig. 2. An illustration of full thermocycle tests setup (the uni-couple, the homemade rig for stability tests and the temperature range the thermal cycles were conducted).

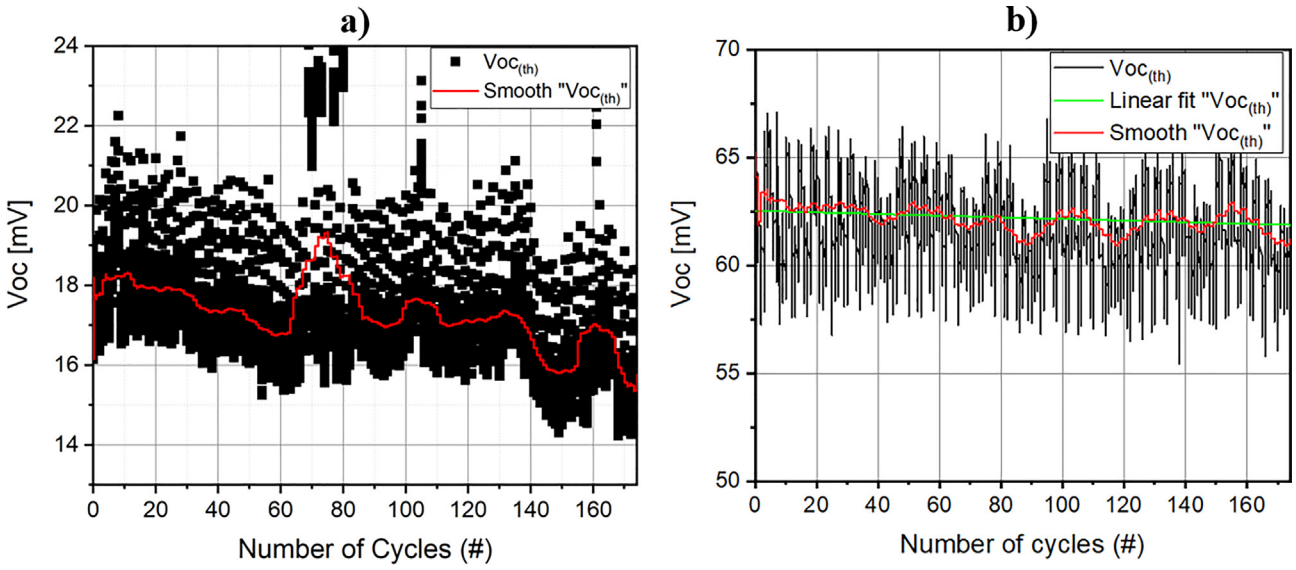

Fig. 3. The thermal open circuit voltage (Seebeck voltage) recorded over time (module 2), plotted against the number of cycles (in black), the red curve shows the "adjacent averaged Voc_{th}" trend, which shows the decrease of Voc_{th} over time, for the voltage recorded: a) at 200 °C and b) at 400 °C. (For interpretation of the references to colour in this figure legend, the reader is referred to the web version of this article.)

and sintered by different partners (Elkem, Sintef, and UiO) in Thermoelectric Silicides (TESil) project. HMS was synthesized by melting (in an induction furnace) and casting in a graphite mould. From the cast ingots, powder was produced by ball milling down to micro-size powder, using a Herzog HSM 100 vibratory mill and a Planetary Ball mill 100. Furthermore, the powder was consolidated into pellets by Spark Plasma Sintering (SPS) (Dr. Sinter, SPS-825). However, MGS was synthesized through solid state route and pelletized by conventional Hot Pressing (HP) (home made at the University of Oslo-Norway). Further thorough details from materials modelling, powder synthesis and pellet consolidation are not yet public as it is still an ongoing project. Pellets of 20–36[mm] diameter and 5 mm height, for the HMS and MGS were cut using a Minitom (Struers) equipped with a diamond saw (Diamond Cut-off Wheel MOD13, 127 mm (5″) dia. × 0.4 mm × 12.7 mm dia.) into legs of 4x4x3[mm] (±50μm dimensions after cutting, grinding and polishing steps). Finally, all cubes were ground by silicon carbide up to 2400grit grinding papers and polished in 3 steps using 6μm,3μm and 1μm diamond suspensions (Struers).

As illustrated by Fig. 1, the thermoelectric modules were assembles using silver (Ag) sheet (Sigma Aldrich) of 0.25 mm thick electrode on the hot side and Ag sheet (Sigma Aldrich) of 0.1 mm thick on the cold side. A layer of a conductive silver paste (Sigma Aldrich) was painted at the interface of the electrode-TE leg as bonding material both on the hot side and cold side. For module one, the n- and p-type unicouples were not metallized, while for module two the legs were metallized by 50 nm sputtered Au layer (on both the cold and hot side) using a turbomolecular pumped coater (Q150T, Quorum). Finally, on the hot and cold side alumina (Al_2O_3) sheet was utilized as an electric insulator (to avoid overload) between the heat source and heat sink.

2.2. Performance tests

The Performance and stability tests were conducted on a homemade rig, as shown in Fig. 2 equipped with a DC powered 100 W heater Inconel block (Dalton WattFlex, USA) on the hot side and a water-cooled copper block, with Minichiller 280 (Huber Kältenmaschinenbau AG, Germany) as an external cooler on the cold side. On the rig, one uni-couple is clamped, and pressure applied from top using two springs at both HMS and MGS sides, which respective temperatures are monitored by K-type thermocouples. The Seebeck (thermal) voltage and temperature are acquired using a National Instruments Data Acquisition Module (NI9210), and, the system is equipped with an electronic load form Array (3721A 80 V/40A 400 W), as a current load which also act as a Current-Voltage (IV) data acquisition system. All appliances are automatically controlled virtually via a LabVIEW control system. Skomedal thesis [20] has provided more details on the rig and experimental set-up.

The TE elements' performance is tested under isothermal (isothermal sections are shown in the full temperature program, supplementary S9) and thermal cycle conditions (following the temperature program shown on Fig. 2 above) under ambient conditions. The whole temperature program presented in the supplementary section S9, consists of one isothermal section recorded from 200 °C–400 °C with 50 °C step size and 3 thermocycle sections followed in the test as detailed on the table on the right-hand bottom corner with 3 h holding time per half cycle. The aging tests were recorded in the isothermal sections with 24 h retention time at each temperature on the hot side and the cold side fixed at 20 °C.

2.3. Post-characterization

After the long-term tests, further studies were conducted on the tested legs to investigate the effects of long-term operation on the legs under thermal stresses. The carried-out tests were the Seebeck coefficient and resistivity (where the homemade rigs was used), Vickers microhardness tests (using FutureTech FM-700 with a load of 200 g) and cross-section microstructure analysis (using a Field Emission Scanning Electron Microscope (FE-SEM) equipped with an Electron Dispersive Spectrometer (EDS) detector from JEOL (JSM-7200F)). Particularly, the electrode -TE leg contact regions (both n- and p-types) were the focus of the study. After disassembling the modules, the legs were clipped with metal clips (fixation clips from Struers) and hot mounted in a conductive resin (Polyfast from Struers). The resin cast legs were ground using a similar recipe as in section 2.1, and polished using polycrystalline diamond suspension up to 1μm (DP-Suspension, alcohol based

<0.5%water content – Struers). At the end of every grinding step and polishing step, the pellets (the hot mounted specimen) were cleaned in ethanol and dried using a low-pressure warm air by a hair drier.

3. Results

Performance and stability tests were conducted on two modules for over 25thermocycles in 200 h (on module 1) and over 300 thermocycles in 2200 h (on module 2). At the same time, the thermally generated open circuit voltage ($Voc_{(th)}$) was monitored along the stability tests. Fig. 3 a) and b) shows the $Voc_{(th)}$ plotted against the number of thermocycles in the temperature range of 200 °C–400 °C (module 2), where the $Voc_{(th)}$ is presented as separate reading at 200 °C and 400 °C. The uni-couple experienced 16.5% $Voc_{(th)}$ gradual decrease in the 200 °C–400 °C temperature range after more than 180cycles. Moreover, 115 thermocycles were run at 25 °C–400 °C temperature range, the thermal stress resulted in a reduction of 24.5% of the initial $Voc_{(th)}$ as also represented in supplementary results (S1). The reduction of the open circuit voltage, as reported by other research on HMS and MGS based modules [6] is mostly a result of the module inner resistance increase (with 20% contact resistance share) especially at the interface of the TEM and electrode. Unfortunately, the internal resistance was not measured in this study due to high contact resistance (12Ω initially), which lead to failure to record meaningful current–voltage (IV) data. To reduce the initial contact resistance, extra pressure was exercised on the unicouple, however the resistance could not be further decreased, due to the possibility of breakage of the brittle MGS leg (as it was sintered by hot press). At the end of the tests on module 2, the contact resistance had increased to more than double the initial value up to 26.76Ω, but this was mainly due to mechanical failure, especially on the n-type leg.

Fig. 4 a) and b) represents a cross section of the module one's MGS hot side and cold side interfaces, respectively, after 25 thermocycles from 200 to 400 °C. After the tests, the MGS leg-electrode had a more solid bond at the hot side than on the cold side. The SEM picture of the cross-section in Fig. 4 a) shows that the MGS had a better bond at the electrode-MGS interface, by the visible formation of an interdiffusion layer from diffusion of Sn from the TE alloy and In from the paste. However on the cold side the bond looks decent, though the Sn diffusion is not homogeneous along the interface as it can be noticed on Fig. 4 b). It is possible that the latter lack of homogeneity caused a solid bond in some regions but looser contacts in regions with more Ag. For further understanding, full composition/phase EDS maps can be consulted in the supplementary results on both the hot (supplementary S2) and cold side (supplementary S3) interfaces. It is, important to note (check the S2 and S3 supplementary) that the MGS leg had more physical damages (though anticipated) and oxidation along the grain boundaries which was the major cause of degradation.

In contrast to MGS, the HMS (module 1) contact regions on both hot and cold sides were mechanically weaker after 25cycles. Fig. 4 c) represents the hot side region of the HMS-Ag paste interface and the EDS compositional map (right hand side image) which the back scattered SEM image reveals a thin gap and a thin oxide layer at the interface, respectively. The observed gap is a result of weak adherence of the paste to HMS possibly due to lack of Ag wetting on the HMS surface, which would explain the weak mechanical properties of the bond. In addition, the Ag wetting on the cold side of the p-type leg was far worse than on the hot side (which makes sense). For post-analysis, the contact at the HMS-Ag cold side interface was non-existent which would be justified as an unbalance between the cohesive and adhesive force of the paste, or non-optimal cure conditions (between 140 °C and 150 °C for 30 to 60 min). More EDS analysis are posted in supplementary results (S4), where individual elements are mapped separately.

Fig. 5 shows the module 2, which differs from module 1 by an Au metallization layer of 50 nm to improve the electrical conductivity, increasing the bond wetting and acting as a diffusion barrier at the interface. Stability evaluation was conducted for over 300 thermocycles in 2200 h. On HMS, Fig. 5 a), it can be seen that the metallization layer improved the contact, more on the hot side (left hand side image) than on the cold side (right hand side image). The line scan through the cold side interface reveals a gap that sets the metallization material apart from the TE alloy, however no Au layer could be seen at or across the alloy. This is because at the cold side, the temperature was held at 20 °C and would rise to around 34 °C (as shown on the supplementary results S9) at higher temperatures; hence not enough to prompt diffusion on either side. Moreover, the EDS phase to element ratio and elemental maps (supplementary S5) reveals that at the TE alloy surface a silica oxide is formed at the interface. Though coated and covered by the Ag electrode, the gap at the interface had exposed the HMS surface to an oxidizing agent, where the oxide growth was an additional stress factor that inhibited any chance to bond over time. Similarly, Fig. 5 b) represents the MGS leg from Module 2, with the right and left hand side images representing the hot and cold side interfaces. Apparently, the contact at the hot side looks good, however the Au layer was not seen at the MGS-Ag interface, the main question is, where is the Au layer? The temperature at which the experiments were carried at was too low to melt Au, nevertheless Au has a higher affinity to Ag relative to any phases of the MGS alloy, therefore there is a high probability that Au may have diffused in the Ag paste, and was not detected by the EDS mapping or line scan due to the concentration being below the detection limit.

The cold side interfaces for both legs show poor contact on HMS and mechanical plastic degradation along the MGS-Ag paste interface, cracks were also observed all over the MGS leg. One of the major causes, especially on the electrode-leg interfaces, was the mismatch in coefficients of thermal expansion (CTE), between the components at the interface between the hot side and the legs. The estimated linear thermal expansion for Ag is 19.5 and for Au is 14.2 (μm/mK)) [21], while the estimates for CTEs of the TE legs were computed using a theoretical model for mixtures/alloys by Karunaratne et al. [17] as HMS is 7.89 (μm/mK)), a value which is in accordance to the value published on Mn_4Si_7 by [22] taking dopants under consideration, and MGS is 21.05 (μm/mK) by equation 1–1 using parameters shown in Table 1, the experimental result is nearly the same to the values reported on $Mg_{2.08}Si_{0.4-x}Sn_{0.6}Sb_x$ ($0 \leq x \leq 0.072$) by [23].

The Seebeck coefficient and the microhardness were measured on the legs with Au metallization. The Seebeck coefficient of HMS was found to be 517.5μv/K and that of MGS was +42.3μv/K. It was expected to have a negative Seebeck coefficient for MGS as an n-type semiconductor, but it also had positive regions of the leg. The inhomogeneity of n- and p-type layers in the MGS, at first thought had to be due to the diffusion of Ag and/or Gold in the alloy based on their electronic configurations ([Kr] $4d^{10}$ $5\,s^1$ and [Xe] 4f14 5d10 6 s1, respectively), but the EDS could not prove the presence of Ag or Au based phases in the MGS. However, diffusion of the Sn and Sb from the alloy mainly from the area close to the bonding interface, was the possible cause of the n- and p-type phases in the MGS leg. Furthermore, the Vickers microhardness tests were measured on both metallized legs before and after tests. The microhardness was found to be 556HV and 1000HV before the tests on the n-type leg and p-type legs, respectively. In comparison to the values obtained after the stability tests (322 ± 39HV and

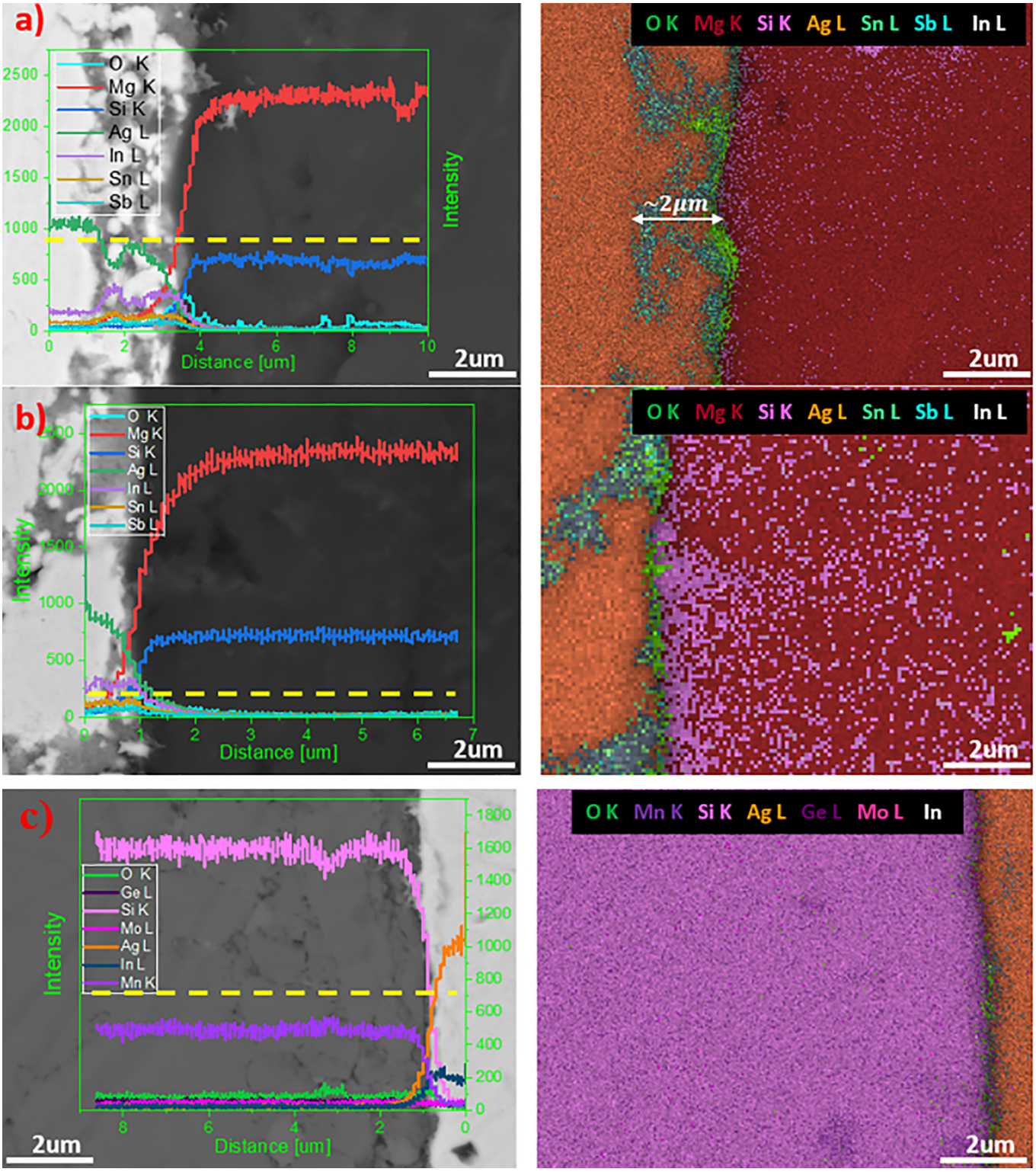

Fig. 4. SEM-EDS line scan and element overlay map of the Ag paste-TE legs (module 1) interfaces, visualized from cross-sections after 25cycles a) MGS-Ag cross-section, where clearly 2 μm visible interdiffusion layer was formed mainly composed of Ag, In, Sn, and Mg corresponding to 34 wt%, 22 wt%, 9 wt%, and 9 wt%, respectively; b) MGS-Ag interface (module 1) at the cold side, where no reaction layer was formed, c) the p-type TE leg (HMS) in module 1, which only a thin layer of silica can be noticed at the interface.

920 ± 37HV, respectively), the MGS experiences 42% reduction, while the HMS was not mechanically affected, and this was confirmed by the back scattered electrons images on SEM.

To summarize, module 1 and module 2 were comparatively discussed, mainly based on the post-stability tests. On both modules the MGS legs (non-metalized and metalized) degraded considerably. As discussed in the previous paragraph, the CTE mismatch may have played a role in the degradation, however the density/-porosity of the MGS legs also facilitated and promoted oxidation of the legs. Based on the second module the metallization reduced

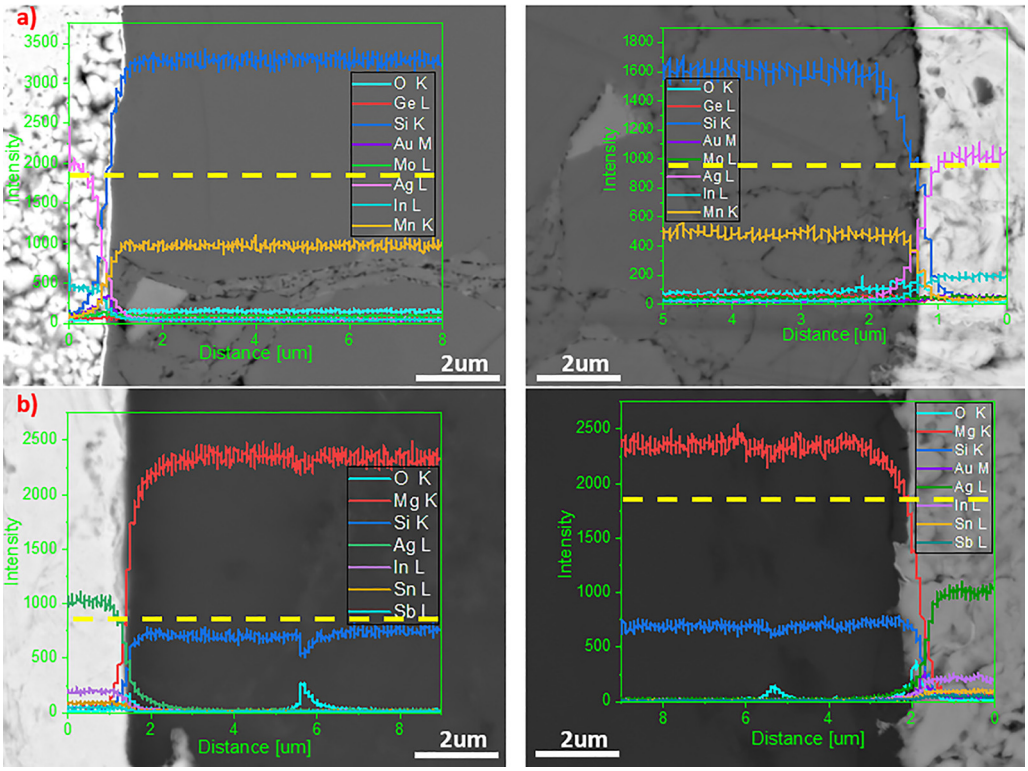

Fig. 5. SEM-EDS representation of the module 2, HMS and MGS legs after more than 300cycles: a) A line scan across the Ag paste -HMS interface at the hot side of the module. The SEM back scattered image shows a long bright strip of Au and a homogeneous Ag paste on the left surface and an unreacted HMS on the left-hand side is the cold side of HMS which shows poor contact and no metallization layer. b) EDS line scan analysis across the hot and cold side of the MGS leg revealing that no Au was still present at the hot side region, though present at the cold side.

Table 1
The parameters used to approximate the CTE of the MGS and HMS alloys.

Phases	$Mg_{2.05}Sn_{0.5}Si_{0.485}Sb_{0.015}$			$Mn_{0.98}Mo_{0.02}Si_{1.73}Ge_{0.02}$				CTE [um/mK]
	wt%	Density [g/cm^3]	CTE [um/mK]	wt%	Density [g/cm^3]	CTE [um/mK]	Ref.	
Mg	43	1.74	25	–	–	–		**21.05**
Si	14	2.32	3	–	–	–	[21]	
Sn	42	7.31	23.4	–	–	–		
Sb	1.4	6.68	10.4	–	–	–		
Mn	–	–	–	51.148	7.43	22		**7.89**
Mo	–	–	–	1.805	10.28	5	[21]	
Si	–	–	–	45.682	2.32	3		
Ge	–	–	–	1.366	5.323	6.1		

diffusion of Sn and Sb as no interdiffusion layer was noticed after more than 2000 h, however the leg still showed mechanical degradation and mixed phases of n- and p-type regions. Meanwhile the HMS legs were mechanically robust. The main drawback was the bonding technique, the legs were expected to form the bond at the beginning of the tests and the method worked for the hot side, though the cold side was badly affected by very low temperatures. The lack of good contact led to oxidation of the TE legs surfaces which weakened the interfaces hindered the bonding possibility. The current research did not examine the extent of oxidation of the MGS (it was discussed based on Skomedal et al. [24] study), but oxidation is believed to be one of the major contributors to degradation of the TE material.

4. Discussion

The Ag bonding material on the non-metalized module (module 1) did not withstand the thermal stresses it was subjected to. This was mainly caused by the wetting of the bonding material and/or the CTE mismatch at the bonding area. The source of less adherence was mainly due to bonding surface oxidation preventing any possible contact between the bonding surface and bonding material. MgO was the main oxide species formed on MGS and SiO_2 (quartz) on HMS; These oxides inhibited the wetting of the bonding material, creating stress related to CTE mismatch (with CTEs, MgO = $10.8 \times 10^{-6}\,K^{-1}$ [25,26]and $SiO_2 = 12.38 \times 10^{-6}\,K^{-1}$ [27]). As discussed in section 3 and represented by EDS map in the supplementary S2, a 2μm layer of Mg-Ag-In-Sn-Sb-O with a 70% In-Sn-Sb rich phase can be seen on the hot side, the CTE of the intermetallic layer formed at the interface ranges between 21 and $22.5 \times 10^{-6}\,K^{-1}$ approximated based on CTEs of alloys published by [28]. It matches well with the CTE of both the silver paste and the TE alloy. However, there has been lack of control of diffusion which could predominantly lead to reducing the CTE in the case of presence of silicon rich phases close to the interface. Similarly, based on the supplementary S3, the cold side followed a similar process trend, though slowly due to temperature difference relative to the hot side. Lastly, both supplementary S2 and S3 show oxide phases across the MGS leg, most of the oxidation is along

cracks and grain boundaries which led to plastic deformation presumably during thermal cycles.

Conversely, with the metallized unicouple subjected to over 300 thermal cycles, the thermal stress after 2200 h had improved electrode-TE leg interface strength both for HMS and MGS. The contact at the hot side of the Au-HMS interface was improved by the increased wettability by Au, though the bond was not mechanically solid, which was caused by lack of intermetallic layer formation between Au, Ag, and HMS. With MGS, the Au metallization slowed down diffusion relative to the module 1 at the hot side of MGS leg interface and had a stronger mechanical bond than HMS. However, the Au layer could not be visualized at the interface as revealed by the SEM images. The disappearance of the Au layer may have been caused by the fact that the MGS leg degraded catastrophically, as it presented deep cracks all over the surface. It is believed that poor mechanical stability was due to the initial consolidation effect on MGS legs. Initially the MGS legs were consolidated by hot press (HP) techniques and was more porous than the SPS compacted HMS, which led to oxidation more on the grain boundaries and ensuing high mechanical degradation. Consolidation by SPS would be much recommended to reduce porosity and increase hardness of the TEM, additionally, based on the HMS hot side bond, it could be seen that the Au wets best at temperature higher than room temperatures for silicides.

The main outcome has been that that the bonding material fits well with the n-type TE material, but not as good with the p-type due to the CTEs mismatch between the two materials. Moreover, it would be better to apply relatively high temperature bonding as is possible with Solid-Liquid interdiffusion (SLID) bonding methods [29] or plasma bonding of the electrodes prior to mounting the stability experiments. The latter would increase mechanical strengths of the bond prior to subjecting the unicouples to mechanical and thermal stresses. On the other hand, it is recommended that the MGS requires consolidation by SPS as hot pressing promotes oxidation of the legs, due to high porosity and brittleness of the legs exposed to thermal stresses.

5. Conclusion

The current study investigated the performance and stability of HMS and MGS based uni-couples with similar electrodes (Ag) and bonding material (Ag) on both hot and cold sides, though distinct from the metallization (Au) on one of the modules. After the stability tests, the HMS legs endured mechanical stress and had improved contact interface with Au metallization relative to the Ag paste alone. However, the MGS leg – module 1, had formed a solid bond with the Ag paste with a reaction layer of 2 μm on the hot side made of Ag-In-Sn ternary phase. The contrary was observed on MGS – module 2; there was no reaction layer observed, but this could have been the difference in exposure time between both modules. Moreover, all MGS legs (module 1 and 2) endured mechanical damages (cracks), which were related to the porosity of the hot-pressed MGS bulk material that promoted oxidation and led to plastic deformation. This work recommends further studies to investigate a combination with SPS consolidated MGS, and finally to find a better bonding material for the HMS with matching CTE.

CRediT authorship contribution statement

Antoine de Padoue Shyikira: Data curation, Conceptualization, Methodology, Investigation, Writing - original draft, Writing - review & editing. **Gustein Skomedal:** Methodology, Supervision, Writing - review & editing. **Peter Hugh Middleton:** Supervision, Writing - review & editing.

Declaration of Competing Interest

The authors declare that they have no known competing financial interests or personal relationships that could have appeared to influence the work reported in this paper.

Acknowledgements

The author would like to acknowledge all partners: Elkem ASA, Sintef, and the University of Oslo (UiO) in TESil project, for their help form material synthesis, pellet consolidation and transport properties tests. We acknowledge financial support from the Research Council of Norway (Project No 269326)

Appendix A. Supplementary data

Supplementary data to this article can be found online at https://doi.org/10.1016/j.matpr.2020.05.193.

References

[1] N. Farahi, C. Stiewe, D.Y.N. Truong, J. de Boor, E. Muller, High efficiency Mg2(Si, Sn)-based thermoelectric materials: scale-up synthesis, functional homogeneity, and thermal stability, RSC Adv. 9 (40) (2019) 22772–23424.
[2] "Lumen learning geology," Lumen, [Online]. Available: https://courses.lumenlearning.com/geology/chapter/reading-abundance-of-elements-in-earths-crust/. [Accessed 30 03 2020].
[3] A. Nozari, P. Norouzzadef, F. Suarez, D. Vashaee, Thermoelectric silicides: a review, Japanese J. Appl. Phys. 56 (May 2017) (2017) 1–27.
[4] A.A. Ivanova, L.D. Baikov, Higher manganese silicide based materials, J. Thermoelectricity 3 (2009) 60–66.
[5] D.M. Row, CRC Handbook of Thermoelectrics, CRC Press, New York, 1995.
[6] G. Skomedal, L. Holmgren, H. Middleton, I.S. Eremin, G.N. Isachenko, M. Jaegle, K. Tarantik, N. Vlachos, M. Manoli, T. Kyratsi, D. Berthebaud, N.Y.D. Truong, F. Gascoin, Design, assembly and characterization of silicide-based thermoelectric modules, Energy Conversion Manage. 110 (2016) 13–21.
[7] H.S. Kim, K. Kikuchib, T. Itoh, T. Iida, M. Tayaa, Design of segmented thermoelectric generator based on cost-effective and light-weight thermoelectric alloys, Mater. Sci. Eng. B 185 (2014) 45–52.
[8] T.P. Generator, Thermoelectric Generator Power Bulk Materials BiTe, PbTe, TEG, [Online]. Available: http://tecteg.com/wp-content/uploads/2015/03/Table-Consisting-of-Various-Thermoelectric-Materials-Researched-for-Power-Generation.pdf. [Accessed 07 12 2017].
[9] T. Nakamura, K. Hatakeyama, M. Minowa, Y. Mito, K. Arai, T. Iida, K. Nishio, Power-generation performance of a pi-structured thermoelectric module containing Mg2Si and MnSi1.73, J. Elec. Mater. 44 (10) (2015) 3592–3597.
[10] J. de Boor, D. Droste, C. Schneider, J. Janek, E. Mueller, Thermal stability of magnesium silicide/nickel contacts, J. Electron. Mater. 45 (10) (2016) 5313–5320.
[11] H. Kaibe, I. Aoyama, M. Mukoujima, T. Kanda, S. Fujimoto, T. Kurosawa, H. Ishimabushi, K. Ishida, L. Rauscher, Y. Hata, S. Sano, Development of thermoelectric generating stacked modules aiming for 15% of conversion efficiency, 24th International Conference on Thermoelectrics, New York, 2005.
[12] N.H. Pham, N. Farahi, H. Kamila, A. Sankhla, S. Ayachi, E. Müller, J. De-Boor, Ni and Ag electrodes for magnesium silicide based thermoelectric generators, Mater. Today Energy 11 (2019) 97–105.
[13] T. Nemoto, T. Iida, J. Sato, T. Sakamoto, T. Nakajima, Y. Takanashi, Power generation characteristics of Mg2Si uni-leg thermoelectric generator, J. Elec. Mater. 41 (6) (2012) 1312–1316.
[14] T. Nemoto, T. Iida, J. Sato, T. Sakamoto, N. Hirayama, T. Nakajima, Y. Takanashi, Development of an Mg2Si Unileg thermoelectric module using durable Sb-doped Mg2Si Legs, J. Electron. Mater. 42 (7) (2013) 2192–2198.
[15] K. Mitra, S. Mahapatra, T. Dasgupta, Fabrication of nickel contacts for Mg2Si based thermoelectric generators via an induction assisted rapid monoblock sintering technique, J. Elec. Mater. 48 (3) (2019) 1754–1757.
[16] W. Liu, S. Bai, Thermoelectric interface materials: A perspective to the challenge of thermoelectric power generation module, J. Materiomics, vol. Article in Press, 2019.
[17] M.S.A. Karunaratne, S. Kyaw, A. Jones, R. Morrell, R.C. Thomson, Modelling the coefficient of thermal expansion (CTE) in MCrAlY bond coatings and Ni based superalloys, J. Mater. Sci. 51 (2016) 4213–4226.
[18] Weishu Liu, Shengqiang Bai, Thermoelectric interface materials: a perspective to the challenge of thermoelectric power generation module, J. Materiomics (2019), https://doi.org/10.1016/j.jmat.2019.04.004.
[19] D.G. Cahill, P.V. Braun, G. Chen, D.R. Clarke, S. Fan, K.E. Goodson, P. Keblinski, W.P. King, G.D. Mahan, A. Majumdar, H.J. Maris, S.R. Phillpot, E. Pop, L. Shi, Nanoscale thermal transport. II, 2003-2012, Appl. Phys. Rev., 1, 011305 (2014); https://doi.org/10.1063/1.4832615, pp. 1-45, 2014.

[20] G. Skomedal, Thermal durability of novel thermoelectric materials for waste heat recovery, The University of Agder - http://hdl.handle.net/11250/2391043, Grimstad-Norway, 2016.
[21] S. MSE, List of Thermal Expansion Coefficients (CTE) for Natural and Engineered Materials, MSE Supplies, 05 09 2019. [Online]. Available: https://www.msesupplies.com/pages/list-of-thermal-expansion-coefficients-cte-for-natural-and-engineered-materials. [Accessed 03 10 2019].
[22] A. Allam, P. Boulet, M.C. Record, Linear thermal expansion coefficients of higher manganese silicide compounds, Phys. Procedia 55 (2014).
[23] P. Gao, I. Berkun, R.D. Schmidt, M.F. Luzenski, X. Lu, P.B. Sarac, E.D. Case, T.P. Hogan, J. Elec. Mater. (2013).
[24] G. Skomedal, A. Burkov, A. Samunin, R. Haugsrud, H. Middleton, High temperature oxidation of Mg2(Si-Sn), Corros. Sci. 111 (2016) 325–333.
[25] Crystran, "Magnesium Oxide (MgO),", Online Available: https://www.crystran.co.uk/optical-materials/magnesium-oxide-mgo 2012 Accessed 18 03 2020.
[26] M.A.S. Rao, K. Narender, Studies on Thermophysical Properties of CaO and MgO by gamma-ray attenuation, J. Thermodyn. 2014 (2014) 1–8.
[27] A. Materials, "Silica - Silicond dioxide," 13 03 2001. [Online]. Available: https://www.azom.com/properties.aspx?ArticleID=1114. [Accessed 18 03 2020].
[28] T. Gancarz, P. Fima, J. Pstrus, Thermal expansion, electrical resistivity, and spreading area of Sn-Zn-In alloys, J. Mater. Eng. Perform. 23 (5) (2014) 1524–1529.
[29] T.A. Tollefsen, A. Larsson, O.M. Løvvik, K. Aasmundtveit, Au-Sn SLID bonding - properties and possibilities, Metal. Mater. Trans. B 43B (2012) 397–405.